

Bayesian Inference of Supernova Neutrino Spectra with Multiple Detectors

Xu-Run Huang,^{a,b} Chuan-Le Sun,^a Lie-Wen Chen,^a Jun Gao^a

^aSchool of Physics and Astronomy, Shanghai Key Laboratory for Particle Physics and Cosmology, and Key Laboratory for Particle Astrophysics and Cosmology (MOE), Shanghai Jiao Tong University, Shanghai 200240, China

^bDepartment of Physics, The Chinese University of Hong Kong, Shatin, N.T., Hong Kong S.A.R., China

E-mail: xr-huang@cuhk.edu.hk, chlsun60@sjtu.edu.cn, lwchen@sjtu.edu.cn, jung49@sjtu.edu.cn

Abstract. We implement the Bayesian inference to retrieve energy spectra of all neutrinos from a galactic core-collapse supernova (CCSN). To achieve high statistics and full sensitivity to all flavours of neutrinos, we adopt a combination of several reaction channels from different large-scale neutrino observatories, namely inverse beta decay on proton and elastic scattering on electron from Hyper-Kamiokande (Hyper-K), charged current absorption on Argon from Deep Underground Neutrino Experiment (DUNE) and coherent elastic scattering on Lead from RES-NOVA. Assuming no neutrino oscillation or specific oscillation models, we obtain mock data for each channel through Poisson processes with the predictions, for a typical source distance of 10 kpc in our Galaxy, and then evaluate the probability distributions for all spectral parameters of theoretical neutrino spectrum model with Bayes' theorem. Although the results for either the electron-neutrinos or electron-antineutrinos reserve relatively large uncertainties (according to the neutrino mass ordering), a precision of a few percent (i.e., $\pm 1\% \sim \pm 4\%$ at a credible interval of 2σ) is achieved for primary spectral parameters (e.g., mean energy and total emitted energy) of other neutrino species. Moreover, the correlation coefficients between different parameters are computed as well and interesting patterns are found. Especially, the mixing-induced correlations are sensitive to the neutrino mass ordering, which potentially makes it a brand new probe to determine the neutrino mass ordering in the detection of galactic supernova neutrinos. Finally, we discuss limitations and perspectives for further improvement on our results.

Keywords: supernova neutrinos, Bayesian analysis

Contents

1	Introduction	1
2	Supernova neutrinos in detectors	3
2.1	Detector configurations	3
2.2	Neutrino spectra and oscillations	5
3	Bayesian inference and numerical results	9
3.1	Basic ideas	9
3.2	Demonstration	11
3.2.1	No oscillation	12
3.2.2	Flavour conversions	15
3.2.3	Impact of cross section uncertainty	18
4	Conclusions	19
A	Flat prior	20

1 Introduction

The epochal detection of neutrino signals of SN 1987A, deriving from the Large Magellanic Cloud (~ 50 kpc), revealed the veil of multi-messenger era of astrophysics. Although only about two dozen neutrinos from this transient were caught by three lucky detectors, namely Kamiokande II [1], Irvine-Michigan-Brookhaven (IMB) [2] and Baksan [3], this detection renders to us the first glimpse into the collapsing core of a dying massive star. After that, various analyses, based on such sparse data, confirmed the outline of stellar core collapse and meanwhile imposed constraints on elusive properties of neutrinos [4–9]. Three decades after that landmark, extraordinary progresses have been made among the modelling of stellar core collapse [10–15], neutrino physics [16] and neutrino detection [17–19]. That is, millions of neutrinos will be detected with unprecedentedly high precision in modern neutrino observatories if the next galactic CCSN exploded at a typical distance of ~ 10 kpc (approximately the distance between the centre of the Milky Way and our Solar System) [20, 21]. Such detection will promise, with no doubt, a much vaster playground for investigating meaningful topics in both CCSN physics and neutrino physics [20–22] (also other potentially interesting topics [23–25]).

Modern hydrodynamic codes are now capable of performing successful simulations of the collapse and explosion of massive stars [12, 26–28]. They enrich our understanding of the explosion mechanism and characteristics of the related neutrino emission [15, 22]. However, a direct confirmation of those models is still missing and thus highly anticipated. Multiple neutrino detectors are currently in operation and scrutinizing the cosmos, or expected to operate in the future. Furthermore, some of them can promise unprecedentedly high statistics if the target is not too far, including water-based Cherenkov detectors (Hyper-Kamiokande [29], IceCube [30]), liquid scintillator detectors (JUNO [31], THEIA [32]), liquid argon time projection chambers (DUNE [33–35]), Pb-based cryogenic detectors (RES-NOVA [36, 37]) and so on. Although it is too complicated to predict when the next CCSN will occur in the

vicinity, a rate of 1.63 ± 0.46 CCSN/100 y is obtained for the Milky Way and galaxies in the Local Group [38]. So, it could be promising to anticipate at least one galactic CCSN during the missions of those contemporary or next-generation detectors.

Such a prospect has attracted quite some attentions on how to maximize the scientific return from such detection in the communities of astrophysics and particle physics. Among them, reconstructing the energy spectrum of neutrinos is significant for physics but demanding for the amount and quality of data. Attributing to the relatively strong interaction and low requirement on detector construction, inverse beta decay on proton (IBD-p) has become the most widely-utilised reaction channel in large-scale neutrino detectors [29, 31, 32]. This literally promises a good sensitivity to electron-antineutrinos. Elastic scattering on electron and charged current reaction on nuclei (e.g. ^{12}C [31], ^{16}O [29] and ^{40}Ar [34, 35]) offer the approaches to catch electron-neutrinos. Previous works have shown that a reasonable precision can be achievable in the measurement of supernova ν_e spectrum [39, 40]. Now, the last task is presented as achieving sufficient sensitivity to heavy flavour neutrinos which can only undergo neutral current processes in such low-energy region. Therefore, elastic scattering on proton (pES) in scintillator detectors has been naturally proposed as an available access to heavy flavour part of supernova neutrinos [41]. Nevertheless, the RES-NOVA project, recently proposed in ref. [36] with the primary mission of detecting supernova neutrinos, promises high statistics via the coherent elastic neutrino-nucleus scattering on Lead. Note that different species of heavy flavour neutrinos are generally indistinguishable from each other since none of their charged companions would emerge with sufficiently large amount in stellar core collapse¹. However, a synergy of reaction channels is indispensable for extracting flavour-depending information (e.g. the collection of IBD-p, elastic scattering on electron/proton and charged/neutral current reactions on nuclei [42–47]).

According to methodology, previous efforts can be schematically divided into two categories: statistical approaches and unfolding processes. Based on certain templates, statistical analysis extracts signals from noisy data with high efficiency, and thus has been usually adopted [39, 40, 42–44]. In such analyses, the profiles of neutrino fluxes are commonly depicted by the sophisticated Garching formula [48], which has been proven to be well compatible with high-resolution simulations [49]. To some extent, this simple fit represents our sophistication on the modelling of stellar core collapse. However, the heavy dependence on this analytic formula may potentially discard some important features of the real signals. Unfolding methods [45–47] are capable of alleviating such drawback, since they do not rely on any analytical formulas. But the shortages of such methods are even more severe. Aside from the complexity, the spectral reversion with response matrix belongs to the case of ill-posed problem, which means that small errors or noise can easily lead to artificial patterns in the results [47]. So, the pragmatic strategy is to implement these two processes complementarily in analysis of supernova neutrinos. They all offer meaningful information, only in different manner. In this work, we employ the Bayesian statistics to perform such evaluations. In the last decades, Bayesian method [50] has been proven to be a powerful tool in questions generally handling uncertainty, including gravitational wave astronomy [51], relativistic heavy-ion collisions [52], astrophysics and cosmology [53, 54], and fields of human activity beyond fundamental physics (e.g. Bayesian networks). Especially, it had already been introduced to the analysis of neutrino signals from SN 1987A [9].

In this paper, we demonstrate the use of Bayes’ theorem to evaluate the spectral param-

¹Thus, ν_x is commonly used to denote one species of heavy flavour neutrinos and so do we. Sometimes, ν_x and $\bar{\nu}_x$ appear simultaneously, then they indicate particles and anti-particles, respectively.

eters for all flavours of neutrinos from a galactic CCSN. At the source, we adopt the time-integrated spectra for each type of neutrinos from a long-term axisymmetric core-collapse simulation which is reported in ref. [40]. Then, the simple adiabatic conversion in the CCSN [55] is applied here to account for the inevitable oscillation effects, including the case of normal mass ordering (NMO) and inverted mass ordering (IMO). We also show the results with no oscillation effects. However, any other neutrino conversion models can also be implemented in principle. As to the detection, we attempt to simultaneously obtain high statistics and full sensitivities to all types of neutrinos by taking advantage of three large-scale neutrino observatories, namely Hyper-K, DUNE and RES-NOVA. It should also be mentioned that the pES channel in JUNO is capable of performing flavour-blind detection with high energy resolution. However, it is reported that the reconstructed ν_e and ν_x spectra suffer from a substantial systematic bias of energy threshold induced by the pES channel’s insensitivity to neutrinos with energy below 20 MeV [46]. Note that the peak is usually located at ~ 10 MeV in the spectrum of supernova neutrinos. Instead, the proposed 1 keV threshold for nuclear recoil energy in RES-NOVA offers the flavour-blind sensitivity to neutrinos with energy above ~ 10 MeV [36]. As a demonstration of our method, we make optimistic assumptions and adopt the RES-NOVA setup in its 3rd phase. Nevertheless, it is worthy to mention that the pES channel in JUNO may provide valuable all-flavour information for other purposes, or contribute useful all-flavour information here if the RES-NOVA detector of this scale was not realised in a realistic measurement. Detailed configurations of these detectors will be discussed later. The fast event-rate calculation tool, *SNOWGLOBES*², is employed to compute count rates for channels in Hyper-K and DUNE, while that for RES-NOVA is done with a code developed by our own³. In section 2, we review the detector characteristics and generate the mock data for further analysis. Aside from the detector responses, noise from Poisson processes is also included in the mock data. In section 3, we demonstrate how the spectral parameters are estimated from the mock data via Bayes’ theorem, and numerical results as well. The effects from cross section uncertainties are estimated. Finally, we conclude this study and discuss the limitation in section 4.

2 Supernova neutrinos in detectors

Before getting into details of Bayesian analysis, we summarise the features of detectors employed in this work and the characteristics of supernova neutrinos. Since no experimental data is available up to now, we calculate the number of expected events in each energy bin for each channels, based on the neutrino fluxes from numerical simulation, and then extract the number of events for analysis from a Poisson distribution with the expected count as average value. How we consider the neutrino oscillation effects is also presented in this section.

2.1 Detector configurations

The primary reaction channels for the selected detectors, namely IBD-p in Hyper-K, charged current reaction on Argon (vAr(CC)) in DUNE and neutral current scattering on Lead (vPb(NC)) in RES-NOVA, are adopted in this study to provide sensitivities to $\bar{\nu}_e$, ν_e and ν , sequentially. We also include the elastic scattering on electron (eES) in Hyper-K, in order to further enhance the sensitivity of this collection to ν_e and ν_x . Note that eES channel have

²*SNOWGLOBES* provides detector responses to many reaction channels (see e.g. ref. [17] for details) and it is available at <https://webhome.phy.duke.edu/~schol/snowglobes/>.

³This code and *SNOWGLOBES* have been integrated in our Bayesian code.

different cross sections to each type of neutrinos, i.e., $\sigma_{\nu_e} > \sigma_{\bar{\nu}_e} > \sigma_{\nu_x}$ ⁴. It is also interesting to mention that neutral current scattering on Argon in DUNE can potentially offer good sensitivity to ν_x , just not yet fully studied [35].

Hyper-K is a next-generation water-based Cherenkov detector which is scheduled to start data-taking in 2027 [56]. Its primary missions include precision measurements on neutrino oscillations, searches for proton decay and observations on astrophysical neutrinos [29]. In this study, we employ two reaction channels in Hyper-K, namely the IBD-p ($\bar{\nu}_e + p \rightarrow e^+ + n$) and eES ($\nu + e^- \rightarrow \nu + e^-$). Electrons and anti-electrons are produced in these scatterings and emit Cherenkov lights along with their motions in ultra-pure water. Then, the events can be reconstructed by collecting those Cherenkov photons via photomultiplier tubes (PMT). Currently, the reconstruction of IBD-p event has been well established. Meanwhile, eES event can also get separated from IBD-p signals, to some extent, according to their different angular dependence. Furthermore, it is reported that the neutron tagging efficiency can get improved substantially through addition of gadolinium (e.g., an efficiency of $\sim 90\%$ in a gadolinium-loaded Super-K) [39]. That is, the tagging efficiency for the two reaction channels is expected to be promising since the possibility of gadolinium loading has already been considered in the design report of Hyper-K⁵. Here we just assume a generally full tagging efficiency for the two reactions. On the other hand, according to the design report, the fully configured Hyper-K detector consists of two tanks, of which each contains 258 kton of ultra-pure water. The designed fiducial mass for each tank reaches 187 kton. Therefore, a 374 kton of total fiducial mass for Hyper-K has been adopted in some of previous works (see, e.g., ref. [40, 43]). However, the realistic fiducial mass for one tank can exceed this designed scale and reach 220 kton in the detection of supernova neutrinos, because of the localization in time and the neglect of low energy radioactive background due to the short-time feature of supernova neutrino signals [29]. We thus consider one tank with a fiducial mass of 220 kton, just following the available scale also adopted in ref. [47]. That is, only half of the capability of Hyper-K is under evaluation in this study. As to detector response, we adopt the same smearing matrix and post-smearing efficiency as that of Super-K I (or III, IV), which are provided in *SNOwGLoBES*. Its response corresponds to the assumption of 40% PMT coverage.

DUNE [33, 34] will consist of four time projection chambers which contains 70 kton liquid argon in total. The nominal fiducial mass is 40 kton, and we also adopt this value in this study. However, in principle the available mass may exceed this value when studying supernova neutrinos, just like the case in Hyper-K. The primary goals for DUNE include precision measurements on neutrino oscillation parameters and searching for new physics. Among current-operated and future-planned neutrino detectors, DUNE will bring unique sensitivity to ν_e with energies down to ~ 5 MeV via the $\nu\text{Ar}(\text{CC})$ reaction ($\nu_e + {}^{40}\text{Ar} \rightarrow e^- + {}^{40}\text{K}^*$). When such reactions happen, short electron tracks will be created and recorded, potentially along with gamma-rays in the chambers. DUNE will also have excellent time resolution which assures its capability of precisely depicting the neutrino burst time profile if the source is close enough. For instance, it is possible to identify the neutrino “trapping notch”, which emerges as a consequence of neutrino trapping in the dense collapsing core and typically has a width of 1 – 2 ms, for closest CCSNe (few kpc) [35]. Moreover, in the galactic supernova neutrino detection landscape with DUNE, one of the most interesting topic is that the mass

⁴Strictly speaking, σ_{ν_x} is slightly greater than $\sigma_{\bar{\nu}_x}$ (see figure 2 in ref. [17]).

⁵The project of loading gadolinium into Super-K has already been approved. And this will provide a template for further application in Hyper-K. See ref. [29] for more details.

ordering problem in neutrino oscillations can be decisively determined by the detection of neutronization burst which is almost composed of ν_e when produced [55]. The above works also adopted *SNOwGLOBES* in their studies. Therefore, it is quite convenient for us since the configurations of DUNE has already been provided as well.

RES-NOVA [36, 37] is a newly proposed experiment with the primary aim of hunting neutrinos from CCSNe. It intends to achieve a flavour-blind measurement with low energy threshold, high energy resolution and high statistics to supernova neutrinos, by taking advantage of the large coherent elastic scattering cross sections between MeV neutrinos and Pb nuclei, the ultrahigh radiopurity of archaeological Pb and modern technologies on cryogenic detector. This innovative project carries the ambition of providing a 5σ sensitivity to supernova bursts up to Andromeda. However, the detailed configuration has not been settled yet. In this work, we consider a simple realisation of RN-3 in ref. [36], which is constructed with pure Pb crystals and has a detector mass of 465 ton. It will have a 1 keV energy threshold and a 0.2 keV resolution for nuclear recoil energy. This means that RES-NOVA could be sensitive to neutrinos with energies down to ~ 10 MeV. However, it should be stressed here that we use the observed nuclear recoil energy when handling the data from RES-NOVA, instead of the reconstructed neutrino energy adopted in previous detectors. When neutrinos arrive at the detector, they can possibly undergo the $\nu\text{Pb}(\text{NC})$ processes ($\nu + \text{Pb} \rightarrow \nu + \text{Pb}$). After that, the target nucleus will gain a recoil energy in the magnitude of a few keV, and then billions of phonons will get created in the absorber and act as information carriers. Such experimental strategy can possibly make full use of the entire energies deposited in the detector and lead to a realisation of excellent energy reconstruction. However, unlike the previous detectors, the configuration of RES-NOVA is currently absent in *SNOwGLOBES*. We calculate the event rates following our previous works (i.e., ref. [23, 57]). The averaged neutron skin of Pb nuclei is fixed on the experimental value of ^{208}Pb , namely $R_n - R_p = 0.283 \pm 0.071$ fm from PREX-II [58]. Furthermore, in order to properly account for the effect of threshold, we adopt such an acceptance efficiency function:

$$A(x) = \frac{a}{1 + e^{-k(x-x_0)}}, \quad (2.1)$$

where the values of parameters are taken as $a = 1, k = 5, x_0 = 1.5$. Such arrangements assure that the detection efficiency will swiftly rise up to around 100% from $\sim 0\%$ when nuclear recoil energy goes to 2 keV from 1 keV, and approaches 100% asymptotically after 2 keV. At our estimate, the assumption of a full acceptance efficiency will increase the accuracy of α_{ν_x} by $\sim 16\%$ in the case of no neutrino oscillations, owing to the higher statistics in the energy range below ~ 2 keV, while the impact is merely invisible on the extraction of other parameters. In fact, this function derives from the acceptance efficiency of the COHERENT experiment [59, 60], and can also produce similar structure as the reconstruction efficiency function of DUNE [35], just with different parameters. Note that this efficiency represents a conservative estimate and the real one is yet to be determined.

2.2 Neutrino spectra and oscillations

State-of-the-art stellar evolution theory indicates that dying massive stars would undergo violent core collapse at their end, generating an outward-propagating shock-wave to expel their mantles and exploding as spectacular CCSNe which can emerge as luminous as their host galaxy. In such explosions, almost $\sim 99\%$ of the released gravitational potential energy ($\sim 10^{53}$ erg) will be liberated through neutrino emission. Moreover, the evolutionary histories

of the dense core are imprinted in both the temporal structures and energy spectra of neutrino emissions. Note that the neutrinos can still deliver information out of the collapsing core, even if no electromagnetic signal was emitted due to the formation of black hole in failed CCSN. The detailed characteristics of neutrino emission depend not only on the properties of progenitor star (e.g., mass, compactness and so on [61, 62]), but also on the nuclear equation of state of neutron star which still remains largely uncertain [63–65]. Except that, currently our comprehension on the spectral structure of supernova neutrinos is primarily obtained from studies on numerical simulations, due to lack of experimental data.

According to detailed investigations on supernova neutrino spectra [48, 49], the instantaneous spectrum for each type of neutrinos will generally follow the quasi-thermal distribution (also called Garching formula), which can be presented as

$$f_\nu(E_\nu) = \mathcal{A} \left(\frac{E_\nu}{\langle E_\nu \rangle} \right)^\alpha \exp \left[-(\alpha + 1) \frac{E_\nu}{\langle E_\nu \rangle} \right]. \quad (2.2)$$

Here, E_ν and $\langle E_\nu \rangle$ are the energy and average energy of neutrino in the unit of MeV, respectively; $\mathcal{A} = \frac{(\alpha + 1)^{\alpha+1}}{\langle E_\nu \rangle \Gamma(\alpha + 1)}$ is the normalization factor with Γ being the gamma function; and α characterises the amount of spectral pinching (with large value leading to suppression on high energy tail). α can be determined by the energy moment of the distribution, e.g., the relation

$$\frac{\langle E_\nu^2 \rangle}{\langle E_\nu \rangle^2} = \frac{2 + \alpha}{1 + \alpha}. \quad (2.3)$$

Actually, eq. (2.2) has been usually adopted as well to describe the time-integrated spectra in previous studies [40–44, 66], and so do we. Now, assuming no neutrino oscillation, the flux on the Earth can be expressed as

$$\Phi(E_\nu) = \frac{1}{4\pi d^2} \frac{\mathcal{E}_\nu}{\langle E_\nu \rangle} f_\nu(E_\nu), \quad (2.4)$$

where d is the distance of source, and \mathcal{E}_ν denotes the total energy emitted through a specific species of neutrinos. The spectral parameters for the source, adopted in this work, are given in table 1. It should be mentioned that the progenitor model, used to generate these

Table 1: Spectral parameters for the time-integrated spectra of supernova neutrino fluxes (see table 1 in ref. [40]).

ν	α_ν	$\langle E_\nu \rangle$ [MeV]	\mathcal{E}_ν [10^{52} erg]
ν_e	2.67	14.1	7.70
$\bar{\nu}_e$	3.28	16.3	6.44
ν_x	2.20	17.2	5.88

parameters in the simulation, is expected to explode as one of the most common type II supernova (see ref. [40] for more details).

Now, the predicted event rate for each channel can be calculated. For Hyper-K and DUNE, we set a uniform 100 energy grids to cover the energy range of 0.25 – 100.00 MeV,⁶

⁶A uniform energy grid of 200 bins has been fixed as the highest energy resolution in *SNOwGLoBES*, which covers the energy range of 0.25 – 100.00 MeV.

and drop the first several bins to approximately obtain a threshold of 5 MeV. For RES-NOVA, we also set a uniform energy grid with the bin width of 0.2 keV, which starts from the threshold of 1 keV ⁷. We have also tested another non-uniform grid scheme, i.e., the adaptive energy-gridding technique ⁸ (see ref. [47]), and the results of analysis turn out to be almost the same as that of current grid scheme. With the prediction data, the mock data can be generated now, e.g., given the predicted number of events N_{pd} , the corresponding number N_{md} can be extracted from a Poisson distribution with N_{pd} being the average value ⁹. The results are shown in figure 1. The caveat is that such a treatment means that the mock data is extracted from one simulated measurement. So, it is inevitable that the information reflected by the data may deviates from that of the original source due to the Poisson processes. Only high statistics can alleviate such deviations. However, this is also the fact faced by realistic measurements.

Flavour transitions are also inevitable for supernova neutrinos. These messengers are primarily produced in the dense core of a dying star, penetrate through the thick stellar mantle and ultimately arrive in detectors on the Earth. Various conditions, encountered in this long journey, lead to complex transition patterns, e.g., adiabatic/non-adiabatic transitions, self-induced transitions and earth matter effects [20, 55, 67]. Since this work is not meant to dig into the detail of flavour conversion, we focus on the adiabatic transition associated with smoothly-varying matter potentials in supernovae, for simplicity. On the other hand, the three-flavour neutrino mixing framework has been well established experimentally due to tremendous experimental efforts over the past few decades. So we can describe the flavour transitions in supernovae with proper formulas under specific assumptions. However, there still exist two unknowns up to now in this scenario, i.e., the mass ordering and the complex phase associated with CP-violating observable. For the latter one, previous works have shown that it will not cause sizeable modifications to the signals of supernova neutrinos [68, 69]. But the previous one is crucial to the flavour composition of supernova neutrinos in detectors. And that necessitates the consideration of both NMO and IMO in this work.

Assuming the adiabatic Mikheyev-Smirnov-Wolfenstein (MSW) model, in the case of NMO, the observed fluxes (Φ_ν) are composed with the original fluxes (Φ_ν^0) in the following forms [55]:

$$\Phi_{\nu_e} = \Phi_{\nu_x}^0 \quad (\text{NMO}), \quad (2.5)$$

$$\Phi_{\bar{\nu}_e} = \cos^2 \theta_{12} \Phi_{\bar{\nu}_e}^0 + \sin^2 \theta_{12} \Phi_{\bar{\nu}_x}^0 \quad (\text{NMO}), \quad (2.6)$$

where θ_{12} is the mixing angle with the value $\sin^2 \theta_{12} = 0.307 \pm 0.013$ [70]. In the case of IMO, the formulas are rearranged as [55]

$$\Phi_{\nu_e} = \sin^2 \theta_{12} \Phi_{\nu_e}^0 + \cos^2 \theta_{12} \Phi_{\nu_x}^0 \quad (\text{IMO}), \quad (2.7)$$

$$\Phi_{\bar{\nu}_e} = \Phi_{\bar{\nu}_x}^0 \quad (\text{IMO}). \quad (2.8)$$

And the total fluxes are conserved in both cases with such an equality:

$$\Phi_{\nu_e} + \Phi_{\bar{\nu}_e} + 4\Phi_{\nu_x} = \Phi_{\nu_e}^0 + \Phi_{\bar{\nu}_e}^0 + 4\Phi_{\nu_x}^0 \quad (\text{NMO\&IMO}). \quad (2.9)$$

⁷Such arrangement corresponds to a non-uniform energy grid on neutrino energy with the largest bin width being 0.94 MeV.

⁸In practice, we modify the adaptive energy-gridding technique, especially in the low-energy region, before it is implemented in our analysis. To be more specific, the similar strategy, used to handle the energies above the peak, has been applied to deal with the energies below the peak. Because we believe a proper treatment of the low energy part is quite necessary in order to achieve a better precision.

⁹Such strategy has already been used in previous works, e.g., see ref. [43].

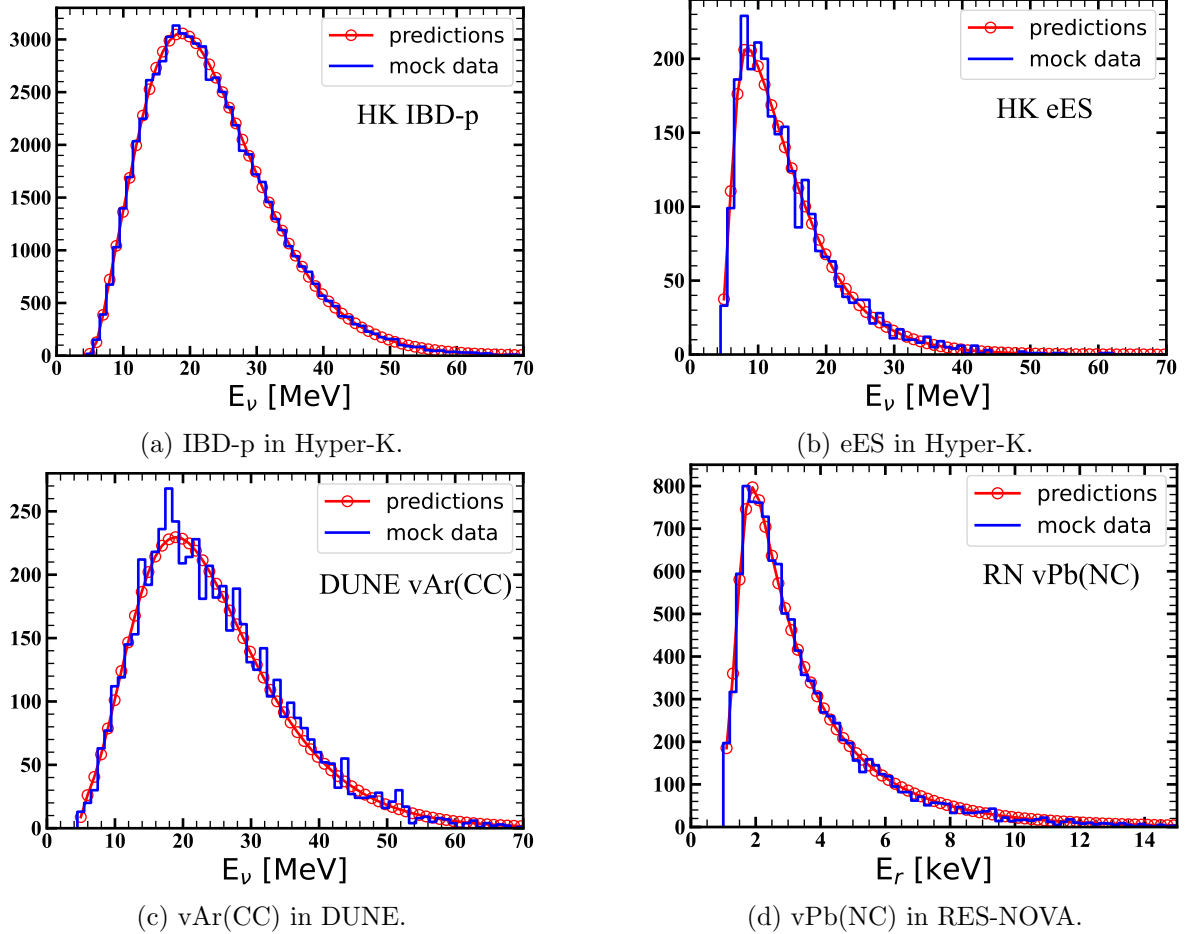
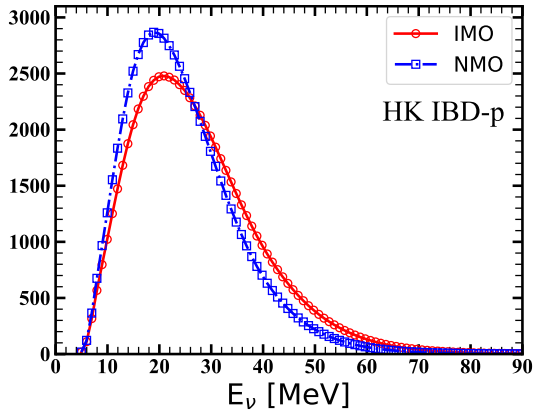


Figure 1: Predicted events and mock data for each reaction channel in Hyper-k, DUNE and RES-NOVA. E_ν and E_r are the reconstructed neutrino energy and nuclear recoil energy, respectively. The source is assumed to be located at a typical distance, i.e., $d = 10$ kpc, and no oscillation effect is under evaluation.

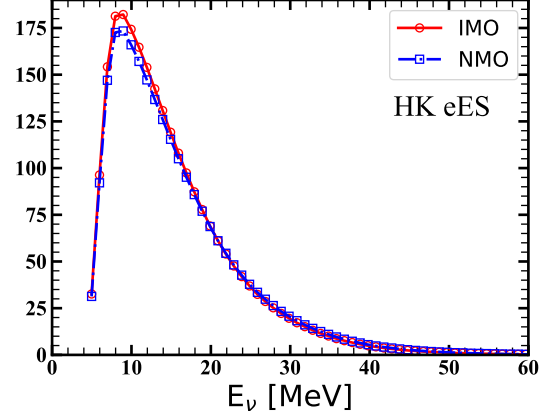
Here Φ_{ν_x} and $\Phi_{\bar{\nu}_x}$ represent the fluxes of neutrinos and anti-neutrinos with heavy flavours, sequentially, and are all equal to one quarter of the total heavy flavour flux. In the data analyses, we do not distinguish between them. From the above expressions, one can see that in the NMO case, the ν_e component is ultimately coming from the original ν_x component while the $\bar{\nu}_e$ flavour is only partially transformed. In the IMO case, the transformations is almost reversed, i.e., the $\bar{\nu}_e$ flavour is fully transformed now while the ν_e component is partially transformed. Note that, instead of simply reversion, the extents of partial transformations are different for the two cases.

The oscillation effects on the prediction of each reaction channel are shown in figure 2. As one can see, it is clear that the predicted energy spectra for different mass ordering diverge from each other in the flavour-sensitive reaction channels, including IBD-p and eES in Hyper-K and $\nu\text{Ar}(\text{CC})$ in DUNE, while they totally overlap with each other in the flavour-blind reaction channel, i.e., $\nu\text{Pb}(\text{NC})$ in RES-NOVA. It is also interesting to mention that the different gaps between IMO and NMO in IBD-p and $\nu\text{Ar}(\text{CC})$ reflect the different extents of partial transformations. For the mock data used in the final analysis, we conduct the same

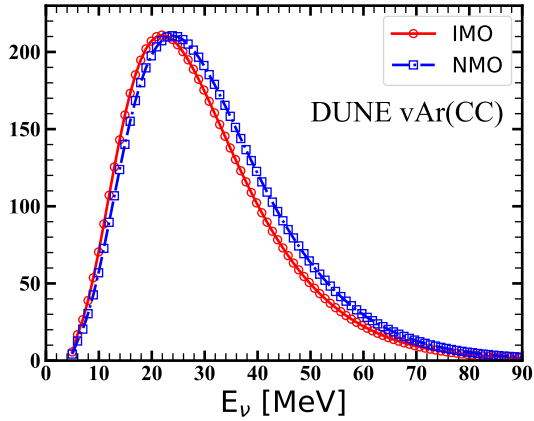
extractions, only including all those ingredients this time.



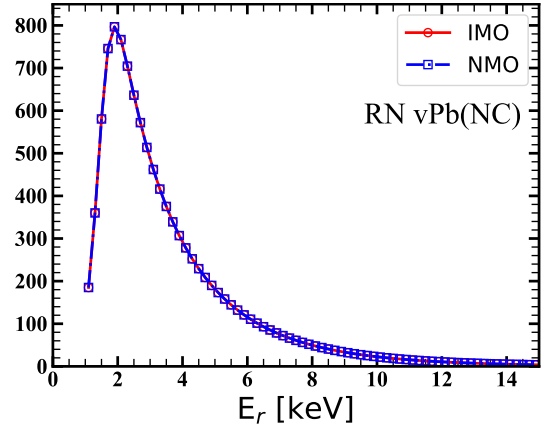
(a) IBD-p in Hyper-K.



(b) eES in Hyper-K.



(c) vAr(CC) in DUNE.



(d) vPb(NC) in RES-NOVA.

Figure 2: Predicted events in each reaction channel under inverted mass ordering (IMO) or normal mass ordering (NMO). E_ν (E_r) denotes the reconstructed neutrino energy (nuclear recoil energy). The distance is assumed to be 10 kpc. The mock data for each case can be extracted with the same strategy in figure 1 and we did not show them here.

3 Bayesian inference and numerical results

Now data analysis can be performed with Bayesian inference to the mock data generated in the previous section. We firstly describe the basic ideas of Bayesian inference briefly and the prior arrangements of our analysis. Then what's following are the demonstration of numerical results and some discussions as well.

3.1 Basic ideas

Bayesian statistics is fundamentally different from conventional frequentist statistics. In Bayesian probability theory, probability is treated as a subjective concept which depends on our state of knowledge, instead of the objective limit of relative frequency of the outcome. So, it is allowed to get updated on the basis of new information which can be collected via some approaches, e.g., conducting experiments. With a full understanding of the issue

under investigation, in principle the Bayesian probability will arrive at a stable value. The basic logical rule which allows us to do such updating is the Bayes' theorem, which can be presented as

$$P(\theta|D) \propto P(D|\theta)P(\theta). \quad (3.1)$$

In the case of parameter estimation, θ and D represent the model parameter to be estimated collectively and the dataset relevant to the model, respectively. The quantity to be evaluated is the posterior probability, $P(\theta|D)$, which stands for the probability of θ given the new dataset D . $P(\theta)$ is the prior probability which quantifies our beliefs on θ before inclusion of new conditions. The likelihood function $P(D|\theta)$ is a mathematical function of θ for a fixed dataset D (also denoted by $\mathcal{L}(\theta; D)$). It quantifies the probability of the observation of D when given the specific parameter θ . In this framework, the main task of inference will get descended into how to calculate the distribution of posterior probability, once the expressions of prior and likelihood are settled. Note that a proper realization of prior probability will be quite helpful in the analysis of less informative dataset, but, somehow, trivial in the case with dataset informative enough.

In this work, since the Garching formula is adopted to describe the time-integrated spectra of supernova neutrinos, we get 9 model parameters, i.e.,

$$\vec{\theta} = (\alpha_{\nu_e}, \alpha_{\bar{\nu}_e}, \alpha_{\nu_x}, \langle E_{\nu_e} \rangle, \langle E_{\bar{\nu}_e} \rangle, \langle E_{\nu_x} \rangle, \mathcal{E}_{\nu_e}, \mathcal{E}_{\bar{\nu}_e}, \mathcal{E}_{\nu_x}). \quad (3.2)$$

The realisation of $P(\vec{\theta})$ could be nontrivial. Generally speaking, the posterior distribution of previous inference can act as the prior distribution of new inference with new information. However, this is not the case in this study, due to the highly limited information provided by the measurement of SN 1987A. Up to now, our knowledge on this issue is primarily obtained from various simulations. In detail, the values of α are usually varying with time in the range of $2 \lesssim \alpha \lesssim 4$ [48, 49, 71]. For $\langle E_{\nu} \rangle$, the magnitude of ~ 10 MeV exists in almost all simulations and also gets confirmed by the observation of SN 1987A. Furthermore, a neutrino energy hierarchy is emerged as $\langle E_{\nu_e} \rangle < \langle E_{\bar{\nu}_e} \rangle \lesssim \langle E_{\nu_x} \rangle$ in simulations [11, 71]. For \mathcal{E}_{ν} , both simulations and SN 1987A indicate that the total released energy via neutrinos should lie in the vicinity of 3×10^{53} erg. And the ansatz of energy equipartition among different flavours of neutrinos has also been found to be roughly valid in simulations. Based on the above statements, we quantify the prior knowledge with 9 independent Gaussian functions associated with the 9 spectral parameters, i.e.,

$$\log P(\theta > 0) = -\frac{(\theta - \mu)^2}{2\sigma^2} + \text{constant}, \quad (3.3)$$

where we exclude the non-physical negative quadrants. The relevant Gaussian parameters are given in table 2. It must be emphasized here that, with such arrangements, we do not

Table 2: The parameters of Gauss distributions in priors. μ and σ represent the center values and standard deviations, respectively. $\langle E_{\nu} \rangle$ s are in the unit of MeV.

	α_{ν}	$\langle E_{\nu_e} \rangle$	$\langle E_{\bar{\nu}_e} \rangle$	$\langle E_{\nu_x} \rangle$	\mathcal{E}_{ν} [10^{52} erg]
μ	3	12	14	16	5
σ	1	4	4	4	5/3

intend to mean that the spectral parameters of neutrinos from the next galactic CCSN would follow these distributions. It rather expresses such a belief that we are quite confident that

θ will lie within $\mu \pm \sigma$, very sure that θ will lie within $\mu \pm 2\sigma$ and almost certain that θ will lie within $\mu \pm 3\sigma$. Values far beyond these regions are still possible but just not likely to happen since that would break the current theoretical framework. Such priors cover the parameter spaces used in the previous analysis [43] with the regions of 3σ , and meanwhile accommodate strong deviations from the expected values. However, it should be noted again that the posterior will be eventually dominated by the data, instead of the choice of priors, when the dataset is informative enough. As a confirmation, we also conduct the analysis with flat priors, and the comparison is shown in appendix A.

The dataset consists of series of energy bins and related number of events, and we conduct the analysis with such a binned likelihood:

$$\mathcal{L}_\zeta(\vec{\theta}; D) = \prod_{i=1}^{N_{\text{bin}}} \frac{\lambda_i^{n_i}}{n_i!} e^{-\lambda_i}, \quad (3.4)$$

for the reaction channel ζ , where N_{bin} is the number of energy bins, λ_i and n_i represent the number of events related to the i th bin in predictions and mock data, respectively. λ_i is a function of $\vec{\theta}$, while n_i belongs to D . Such a Poisson distribution is also adopted in previous studies [43, 44]. Now, the eventual likelihood is simply expressed as

$$\mathcal{L}(\vec{\theta}; D) = \prod_{\zeta \in \text{all exp.}} \mathcal{L}_\zeta(\vec{\theta}; D), \quad (3.5)$$

after combining all the reaction channels. Other potentially useful reaction channels can also be considered via this formula in the future. Furthermore, eq. (3.4) can be replaced with another more well-constructed likelihood, which considers other uncertainties in realistic measurements thoroughly, in future studies.

The calculation of posterior distribution used to be the most complicated part of Bayesian inference. However, powerful methods and tools are currently available to alleviate it. In this work, we implement the ensemble sampler tool, *emcee*¹⁰ [72], to sample the 9-dimension posterior distribution. The *emcee* package is a Python implementation of the Metropolis–Hastings (M–H) algorithm¹¹, which has already been adopted in many published projects in the astrophysics literature. The caveat, which derives from the M–H algorithm, is that the samples initially generated in the chain can be heavily influenced by the choice of starting point in parameter space, due to the inevitably existing correlation among neighboring samples. So, in practice the initial part will be excluded. In this study, we just drop the initial 200 samples in each chain, to obtain sets of stable samples.

3.2 Demonstration

Finally, we perform the analysis and show the numerical results in this section. As a start, we test the capability of our method with the case considering no oscillation effects. So as to obtain an appropriate determination of the posterior distribution, we draw a dataset including 10^6 samples, and calculate the distribution of each parameter by conducting marginalization over other parameters which follows the law of total probability. Then, the cases of different oscillation models are evaluated through the same processes. Among them, $d = 10$ kpc is

¹⁰<https://emcee.readthedocs.io/en/stable/index.html>.

¹¹The M–H algorithm is the most commonly used Markov chain Monte Carlo algorithm (see ref. [50, 72] for more details).

adopted as the default distance of source. In practice, it is possible for this distance to be much smaller, e.g., nearby core collapse supernova candidates reported in [73], including the famous Betelgeuse. Generally speaking, smaller distance means higher statistics and then better precision, when neutrino flux is not too intense to cause signal pile-up in the detector. However, it would be another topic, for future works, on how to properly deal with the effects of signal pile-up if the source is too close. As a test, we only estimate the distance effect in the case of $d = 5$ kpc here.

3.2.1 No oscillation

Figure 3 shows the posterior distributions when no neutrino oscillation is considered¹². The 1-dimension (1-D) distributions for all spectral parameters are plotted on the diagonal. We also present the representative values of these 1-D distributions, i.e., the maximum *a posteriori* (MAP) estimate and the 2σ credible intervals in the highest posterior density scheme, in table 3. As one can see, the three parameters for $\bar{\nu}_e$ flux are constrained quite well in this analysis. In detail, the 2σ symmetrized fractional uncertainties¹³ reach $\pm 2.8\%$, $\pm 0.8\%$ and $\pm 0.9\%$ for α , $\langle E \rangle$ and \mathcal{E} , sequentially. Such high precision is primarily attributed to the ultra-high statistics provided by the IBD-p channel in Hyper-K, as can be seen in figure 1a. Meanwhile, the sensitivity to ν_e mainly derives from the $\nu\text{Ar}(\text{CC})$ reaction in DUNE and the eES channel in Hyper-K. Modest uncertainties are also achieved as $\pm 12.4\%$, $\pm 4.3\%$ and $\pm 4.9\%$. However, the precision for ν_x flux is relatively poor and the fractional uncertainties are only obtained as $\pm 33.4\%$, $\pm 10.7\%$ and $\pm 10.9\%$. The $\nu\text{Pb}(\text{NC})$ reaction in RES-NOVA renders the primary sensitivity to ν_x and also achieves a number of total events even larger than the sum of that from the eES channels in Hyper-K and the $\nu\text{Ar}(\text{CC})$ channel in DUNE. However, the fact is that $\sim 1/3$ of the signals in RES-NOVA come from the ν_e and $\bar{\nu}_e$ fluxes. That is, the information of ν_x from RES-NOVA is actually contaminated. Nevertheless, higher statistics will further improve the accuracy, e.g., enlarging the fiducial mass of RES-NOVA by 10 times will improve the accuracy by $\sim 50\%$ in our test. On the other hand, due to the strong suppression of Pb nuclei on the nuclear recoil energy, a threshold of 1 keV in nuclear recoil energy only makes RES-NOVA sensitive to neutrinos with energy above ~ 10 MeV. Such threshold, although literally quite low among detectors in the same category, is nevertheless not low enough for precision measurement of the spectrum of ν_x flux in supernova neutrinos, since the information below and even in the peak is lost. Such loss naturally jeopardizes precision extraction of information related to spectral shape.¹⁴

On the other hand, the off-diagonal plots suggest the correlations between parameters. Generally speaking, it is quite noticeable that significant correlations appear among parameters in the same type of neutrinos universally, and also only exist among them. Furthermore, these correlations even show certain features for a specific type of neutrinos, i.e., strong positive correlation between α and $\langle E \rangle$ of whom both determine the shape of spectrum, and noteworthy negative correlations between \mathcal{E} and one of the above spectral shape parameters,

¹²*corner* is used to plot such diagrams [74].

¹³Indeed, asymmetries appear among these 1-D distributions in figure 3 and also in table 3, and will also show up in that of other cases. For simplicity, the symmetrized fractional uncertainties are calculated by averaging the positive and negative uncertainties over the most probable values here and after.

¹⁴In the test analyses, we assume a ~ 6 MeV threshold of neutrino energy (i.e., 0.4 keV threshold of nuclear recoil energy) for RES-NOVA, and the accuracy for ν_x is improved by a factor of 1/4. The neutral current scatterings on ^{16}O in Hyper-K can also provide information on the low energy region (e.g., ~ 400 events in the energy range of $5 \sim 10$ MeV). The inclusion of this reaction also lead to a moderate improvement ($\sim 25\%$) on the accuracy of α_{ν_x} .

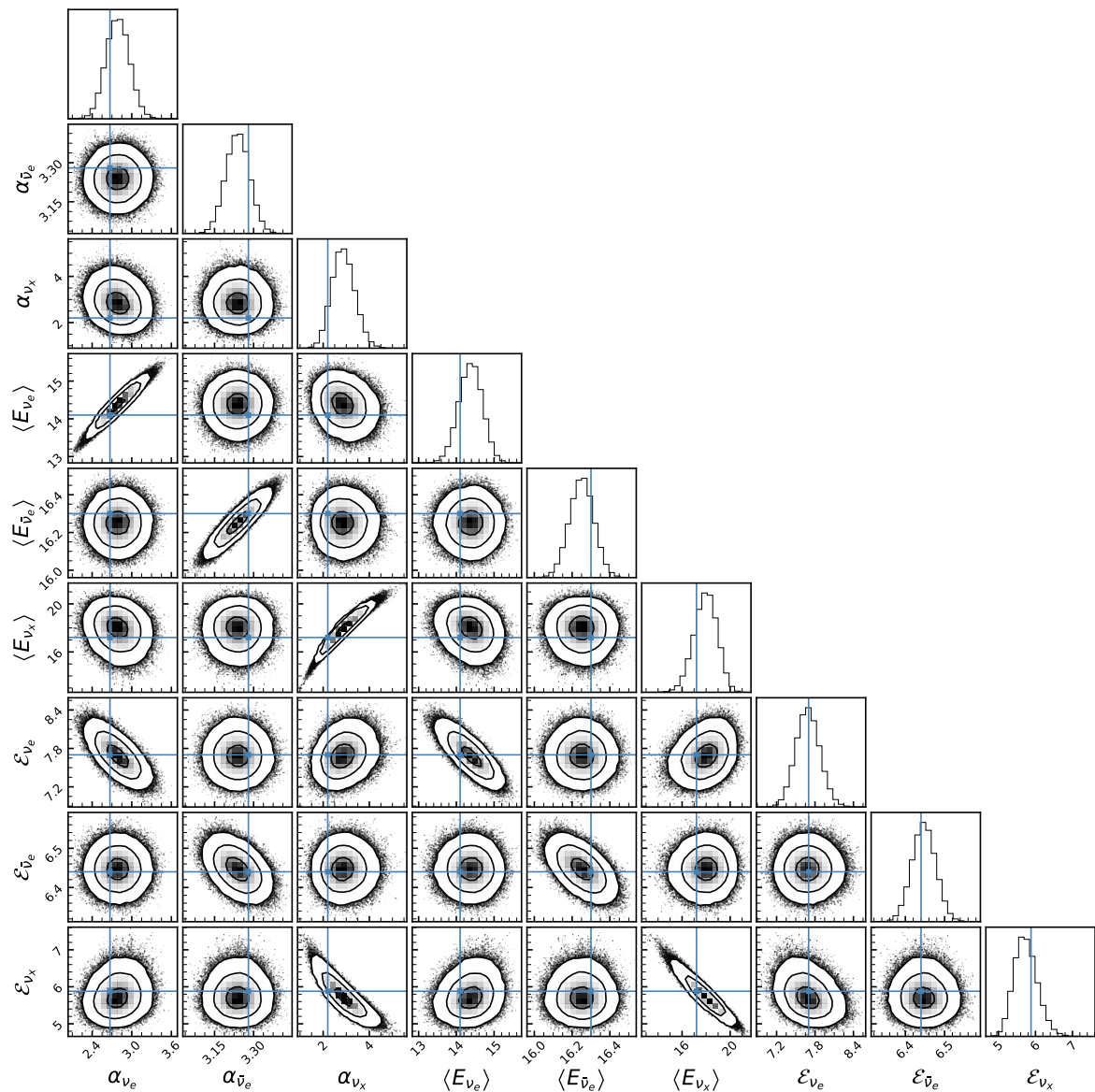


Figure 3: Posterior distributions for the no oscillation case. The Gaussian prior distributions are functioning here. Plots on the diagonal show posterior distributions for the corresponding parameter after marginalization over other parameters, and the off-diagonal ones show correlations between them. Contours in the off-diagonal plots demonstrate the area of 1σ , 2σ and 3σ credible level, respectively. The blue lines mark the parameter values to generate the mock data used in this analysis.

Table 3: The representative values of 1-D posterior distributions. NO indicates the case without neutrino oscillation, while NMO (IMO) represents the case of normal (inverted) mass ordering. Gaussian priors are adopted in all cases. The rows denoted with MAP give the most probable values of the posteriors, while $(2\sigma^-, 2\sigma^+)$ show the relative credible intervals at the 2σ level of probability. % rows give the corresponding symmetrized fractional uncertainties. Meanwhile, %(csu) rows show the estimated symmetrized fractional uncertainties after including a $\pm 5\%$ uncertainty on the cross section of $\nu\text{Ar}(\text{CC})$ reaction in DUNE.

Osc	estimate	α			$\langle E \rangle$ [MeV]			\mathcal{E} [10^{52} erg]		
		ν_e	$\bar{\nu}_e$	ν_x	ν_e	$\bar{\nu}_e$	ν_x	ν_e	$\bar{\nu}_e$	ν_x
NO	MAP	2.83	3.25	2.93	14.37	16.26	17.88	7.71	6.45	5.63
	$2\sigma^-$	-0.38	-0.10	-1.00	-0.63	-0.14	-1.81	-0.41	-0.07	-0.46
	$2\sigma^+$	+0.32	+0.08	+0.96	+0.61	+0.12	+2.02	+0.34	+0.05	+0.77
	%	12.4	2.8	33.4	4.3	0.8	10.7	4.9	0.9	10.9
	%(csu)	13.3	2.8	38.6	4.7	0.8	12.9	8.9	1.0	14.7
NMO	MAP	3.48	3.12	2.37	13.84	16.09	17.45	7.95	6.46	5.86
	$2\sigma^-$	-1.33	-0.16	-0.25	-1.94	-0.25	-0.60	-1.72	-0.13	+0.24
	$2\sigma^+$	+1.81	+0.19	+0.25	+2.27	+0.28	+0.73	+2.16	+0.14	+0.25
	%	45.1	5.6	10.5	15.2	1.6	3.8	24.4	2.1	4.2
	%(csu)	47.3	6.2	11.8	20.4	1.8	4.3	34.6	3.9	8.4
IMO	MAP	3.41	3.85	2.18	15.04	16.03	17.17	7.77	6.58	5.89
	$2\sigma^-$	-0.96	-1.74	-0.07	-1.39	-2.95	-0.18	-0.86	-1.46	-0.06
	$2\sigma^+$	+1.23	+1.57	+0.07	+1.43	+2.03	+0.15	+0.84	+1.88	+0.05
	%	32.1	43.0	3.2	9.4	15.5	1.0	10.9	25.4	0.9
	%(csu)	34.4	46.1	3.7	12.0	19.3	1.0	20.5	35.9	0.9

respectively. Such correlation patterns are primarily embedded in the parameterization of neutrino spectrum (see eq. (2.2) and eq. (2.4)). It is also potentially interesting to mention that such correlations are the weakest for the $\bar{\nu}_e$ flavour while that of the others are comparable¹⁵.

The distance effect is tested here. For a closer source with $d = 5$ kpc, the higher statistics in data lead to better accuracies on the reconstructed spectral parameters, while almost no effect on the correlations among these parameters. In detail, the symmetrized fractional uncertainties are updated by $\pm 6.4\%$, $\pm 2.3\%$ and $\pm 2.6\%$ for ν_e flavour, $\pm 1.5\%$, $\pm 0.4\%$ and $\pm 0.5\%$ for $\bar{\nu}_e$ part and $\pm 20.1\%$, $\pm 6.3\%$ and $\pm 5.8\%$ for ν_x component. However, as a result for comparison, these percentages are calculated with new 2σ credible intervals (i.e., for $d = 5$ kpc) and the most probable values in the previous case (i.e., for $d = 10$ kpc). Such treatment is also applied in similar comparisons hereafter. In short, the accuracies are universally enhanced by $40\% \sim 50\%$ among all parameters in this test.

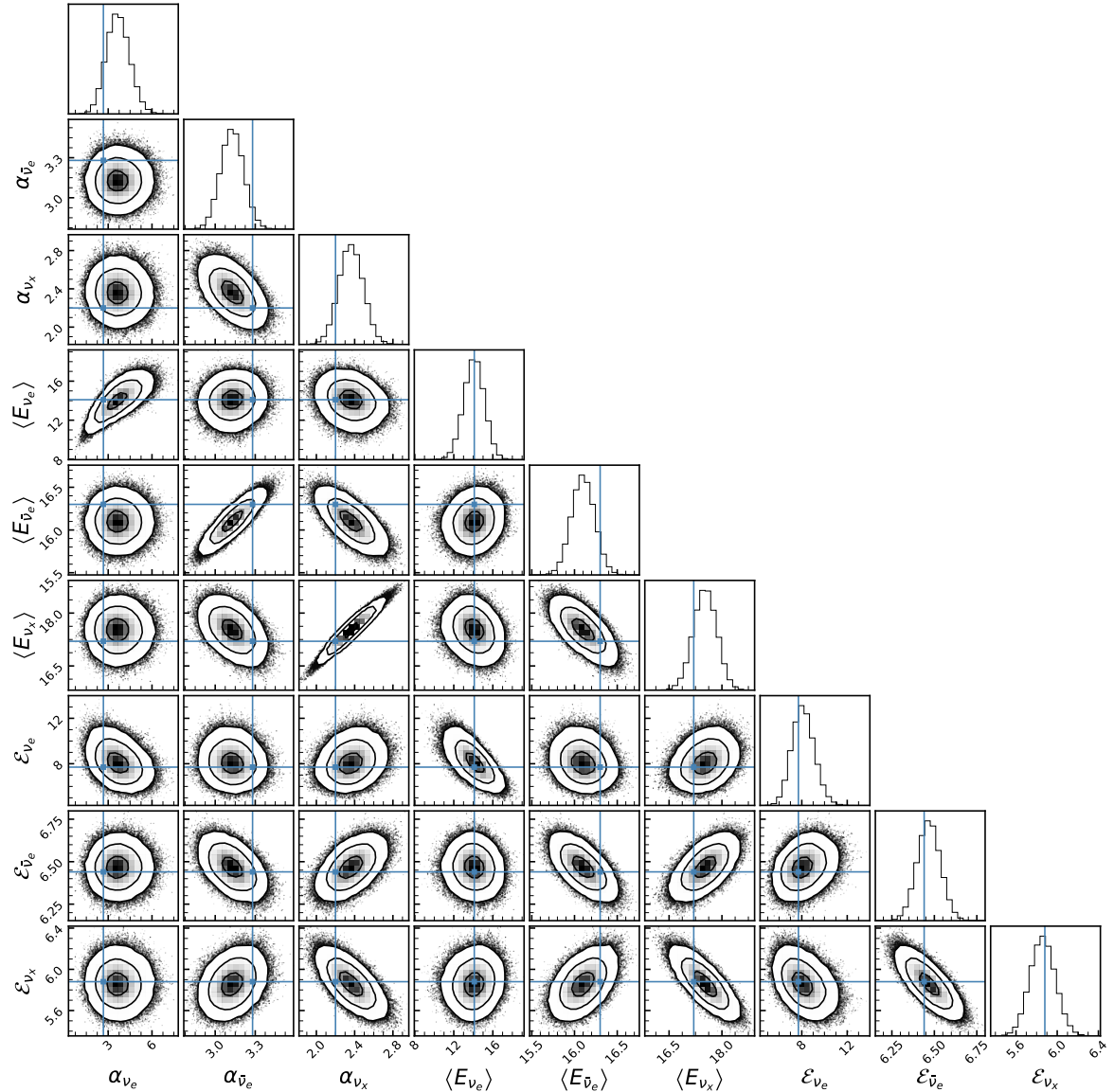


Figure 4: The same as figure 3, but the oscillation effects with normal mass ordering are under evaluation.

3.2.2 Flavour conversions

Figure 4 displays the posterior distributions when the oscillation effects are considered under the assumption of NMO. The representative values, corresponding to the distributions on the diagonal, are also given in table 3. Still, the best results are obtained for the $\bar{\nu}_e$ flavour for the same reason as the case without oscillation effect. Numerically speaking, the symmetrized fractional uncertainties are $\pm 5.6\%$, $\pm 1.6\%$ and $\pm 2.1\%$ for α , $\langle E \rangle$ and \mathcal{E} , sequentially, within a credible level of 2σ . They become worse slightly, due to the partial conversion in eq. (2.6).

¹⁵We swap the parameters of ν_e and $\bar{\nu}_e$ components and such hierarchy still appears, only with the difference between these two species getting decreased by $\sim 50\%$. So it is primarily originated from the detection configurations.

In this flavour conversion mode, the ν_e events and $\sim 30\%$ of $\bar{\nu}_e$ events in detectors are now responsible for the ν_x component. Thus, the results for ν_x component are much better after combining information from all the four channels. The uncertainties are read as $\pm 10.5\%$, $\pm 3.8\%$ and $\pm 4.2\%$, even slightly better than the ν_e results in the case of no oscillation. In contrast, the precision for ν_e are now rather poor, only achieving uncertainties of $\pm 45.1\%$, $\pm 15.2\%$ and $\pm 24.4\%$. Because all the information for ν_e flavour are extracted from the data of $\nu\text{Pb}(\text{NC})$ reactions in RES-NOVA, and only $\sim 1/6$ of these data are responsible. Note that the deviation between posterior and prior distributions for α_{ν_e} is kind of trivial, which means the result get too much information from the prior, instead of the data. It indicates that the constraint on α_{ν_e} is actually quite limited in this case.

The numerical results for the IMO conversion are illustrated in figure 5 and table 3. In this conversion mode, neutrino signals in all reaction channels are mainly coming from the original ν_x component (see eq. (2.7) and eq. (2.8)), which naturally lead to a promising precision in this part. That is, the symmetrized fractional uncertainties are obtained as $\pm 3.2\%$, $\pm 1.0\%$ and $\pm 0.9\%$ for the three parameters correspondingly. It should be mentioned that ν_x components are responsible for $\sim 2/3$ of the total neutrinos. Hence, it is quite significant to achieve such high precision on the measurement of this part. However, the price is large uncertainties on the measurements of other components. The representative values of posterior distributions are $\pm 32.1\%$, $\pm 9.4\%$ and $\pm 10.9\%$ for the ν_e flavour, and $\pm 43.0\%$, $\pm 15.5\%$ and $\pm 25.4\%$ for the $\bar{\nu}_e$ part. The situation of the $\bar{\nu}_e$ part are quite similar to that of the ν_e flavour in the NMO conversion. Similarly, the caveat is that the prior distribution provides too much information in the evaluation of $\alpha_{\bar{\nu}_e}$, also just like the case of α_{ν_e} in the NMO conversion.

Aside from the diagonals, the off-diagonal plots in figure 4 and figure 5 portray the correlations between parameters as 2-dimension distributions. So as to quantify these correlations, the matrices of correlation coefficients, namely \mathbf{V}^{NMO} and \mathbf{V}^{IMO} , are calculated and shown in figure 6, where the value in a coordinate of a matrix refers to the distribution in the same coordinate of posterior charts. Apparently, the correlations among the three parameters of one specific species remain the same and, more specifically, another universal hierarchy among the three correlation coefficients emerges as $|\rho(\alpha, \langle E \rangle)| > |\rho(\langle E \rangle, \mathcal{E})| > |\rho(\alpha, \mathcal{E})|$. Such patterns are still controlled by the spectral formalism. On the other hand, different correlation patterns appear between different oscillation models. In the case of NMO, moderate correlations exist among spectral parameters from $\bar{\nu}_e$ and ν_x components. That is, the spectral shape parameters, α and $\langle E \rangle$, of $\bar{\nu}_e$ flux have negative correlations to the corresponding parameters of ν_x flux, and so do the total energy parameters, \mathcal{E} . This can be expected from the mixing of these two components, as described in eq. (2.6). As a consequence, more complicated correlation patterns stem from two categories of correlations mentioned above (see figure 6a and figure 4 for more details). However, it turns out that no such correlations are seen in the case of IMO, while the mixing of ν_e and ν_x components does exist, i.e., in eq. (2.7). The absence here is ascribed to the different sensitivities to ν_e and $\bar{\nu}_e$ species in our detector configurations¹⁶. Such difference between NMO and IMO can potentially act as another smoking gun to determine the mass ordering in measurement of the next galactic

¹⁶As a test, the exchange of parameters between ν_e flavour and $\bar{\nu}_e$ component is estimated again and the mixing-induced correlations are still missing for IMO while clear for NMO. The effect is that these correlations become relatively weaker in the NMO mode. We also swap the values of $\sin^2 \theta_{12}$ and $\cos^2 \theta_{12}$, and only see some mild effects on the correlation coefficients (even weaker than the previous case).

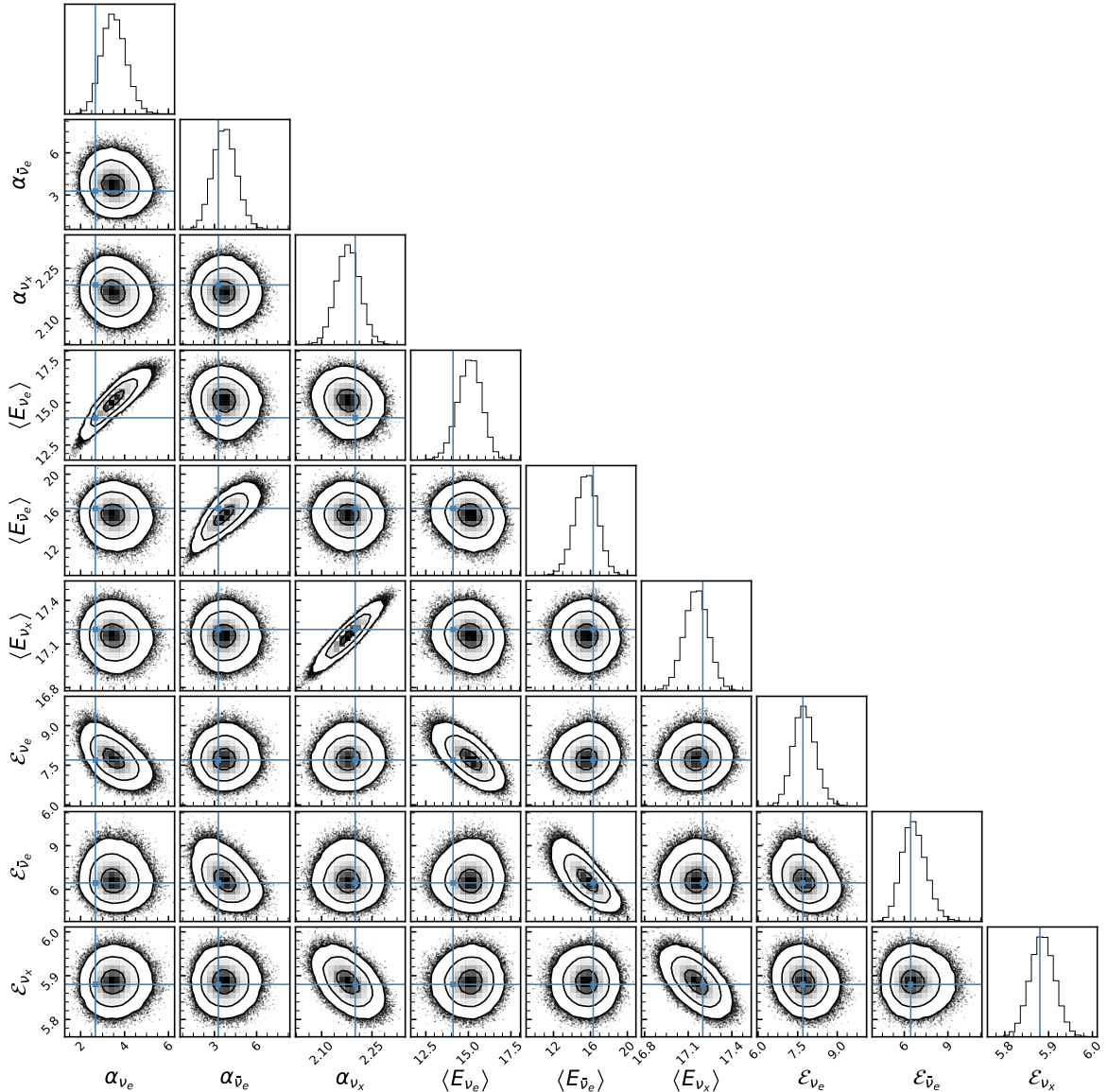


Figure 5: The same as figure 3, but the oscillation effects with inverted mass ordering are under evaluation.

CCSN ¹⁷, although we postpone further estimates in future work.

Again, we check the results for $d = 5$ kpc. The correlation patterns for both NMO and IMO are still robust, only with modest enhancements found in spectral-induced correlation coefficients of the ν_e ($\bar{\nu}_e$) flavour in NMO (IMO) conversion. As to the accuracies of reconstructed parameters, universal improvements of 40% \sim 50% are again obtained for the $\bar{\nu}_e$ and ν_x components in the case of NMO, and for the ν_e and ν_x components in the case of IMO.

¹⁷When analysing the data with NMO template, dataset with IMO will show even stronger mixing-induced correlations than dataset with NMO (e.g., the correlation coefficients between $\alpha_{\bar{\nu}_e}$ and $\langle E_{\nu_x} \rangle$ ($\alpha_{\bar{\nu}_e}$ and E_{ν_x}) in the two cases are shown as -0.78 vs -0.46 (0.64 vs 0.30), and, however, the impacts on different coefficients can be different.). If the analyses were conducted with IMO/NO template, we see no manifest signals or just rather weak trends.

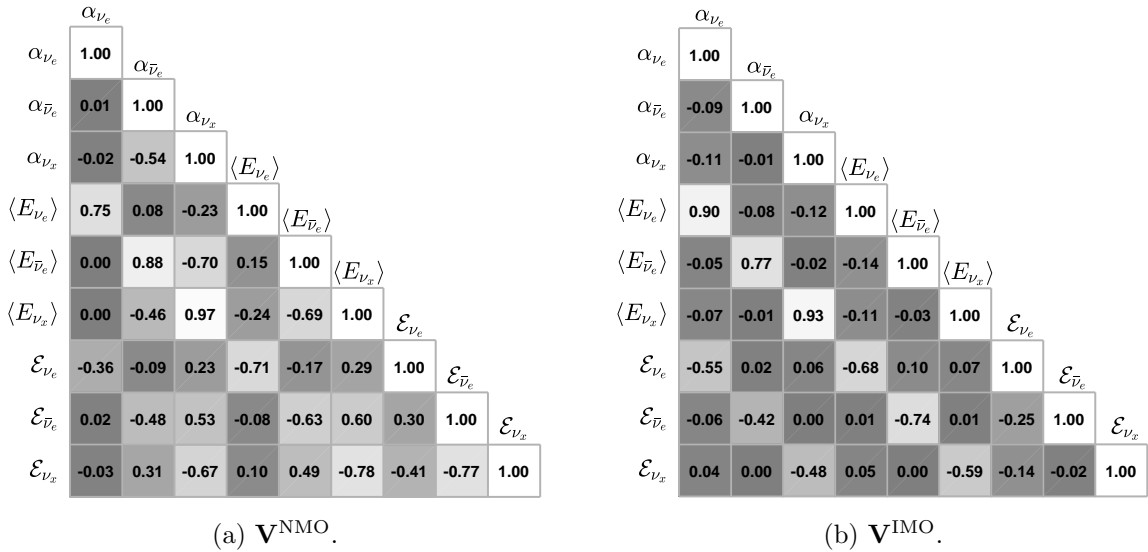


Figure 6: The matrices of correlation coefficients for NMO and IMO.

Nevertheless, different parameters of the ν_e component in NMO conversion show different sensitivities to the change of target distance. That is, the accuracy for \mathcal{E}_{ν_e} is increased by $\sim 45\%$ in such test, while that for $\langle E_{\nu_e} \rangle$ is only enhanced by $\sim 15\%$ and it turns out to be rather weak improvement ($\sim 4\%$) on α_{ν_e} . It is similar for that of the $\bar{\nu}_e$ flavour in IMO conversion. So the measurement of α_{ν_e} ($\alpha_{\bar{\nu}_e}$) in NMO (IMO) conversion deserves further investigation.

3.2.3 Impact of cross section uncertainty

Until now, all the evaluations are performed under an assumption that the cross section for each reaction channel is well determined. However, the fact is not so optimistic. Especially, the cross section for $\text{vAr}(\text{CC})$ in DUNE still have large theoretical uncertainty, e.g., a deviation of almost one order of magnitude between the predictions from QRPA-C calculation [75] and NSM+RPA calculation [76]. Such large theoretical uncertainties will substantially impede the interpretation of such measurements, as reported recently by the DUNE Collaboration [77]. Here, to draw an idea about how this cross section uncertainty would affect our results, we reanalyse the mock data after introducing a scaling factor of $\pm 5\%$ on the previous $\text{vAr}(\text{CC})$ cross section¹⁸. The estimated symmetrized fractional uncertainties are also presented in table 3, just lying below the previous results. Overall, the total emitted energy is the most sensitive one among the three parameters. The effects on the other spectral shape parameters are relatively small. On the other hand, the extraction of neutrino species, which is associated with the data from Hyper-K, will be less influenced by such a cross section uncertainty, since the data from Hyper-K is much more informative than the others. In particular, the results are almost unaffected in our estimate for $\bar{\nu}_e$ flux under no oscillation and ν_x flux under IMO conversion. Interested readers can refer to table 3 for detailed information. In all, it can be seen that even a $\pm 5\%$ uncertainty on the $\text{vAr}(\text{CC})$ cross section would manifestly affect the extraction of neutrino spectral parameters here. And the

¹⁸According to the discussion in Ref. [77], we could expect a statistical uncertainty of 5 – 10% on the total cross section with a ton-scale detector running beside the Spallation Neutron Source for a few years.

almost 100% cross section uncertainty, currently existed, would cause severe biases which make the results not reliable. So it would be invaluable to control the theoretical precision via a direct measurement of this reaction in the future.

4 Conclusions

In this paper, we present the retrieval of energy spectra for all flavours supernova neutrinos with Bayesian inference by combining data from multiple detectors. When selecting reaction channels, the collection of IBD-p and eES reactions in Hyper-K, $\nu\text{Ar}(\text{CC})$ in DUNE and $\nu\text{Pb}(\text{NC})$ in RES-NOVA is employed under the consideration of flavour sensitivity and data statistics. Before analysing the mock data, we quantify the prior knowledge on the energy spectra of supernova neutrinos with modified Gaussian functions. Then, using a Poisson likelihood, we sample the posterior distribution, which has 9 degrees of freedom, and extract the probability distribution of each parameter. Furthermore, the correlation coefficients among parameters are also estimated and discussed.

Assuming a typical source distance (i.e. $d = 10$ kpc) in our Galaxy, our results show that the average energy and individual emitted energy can be determined with an accuracy of a few percent in normal (inverted) mass ordering, except for the ν_e ($\bar{\nu}_e$). Especially, those for heavy flavour neutrinos are reconstructed with a 1% precision under the oscillation effect of inverted mass ordering. The spectral pinching for either $\bar{\nu}_e$ (ν_x) can also be measured to a few percent precision in normal (inverted) mass ordering. In contrast, that for either ν_e or $\bar{\nu}_e$ is hardly extractable from the data, accordingly. Nevertheless, based on the overall accuracy inferred here, it is interesting to mention that the precise determination of neutron skin of Lead should be promising through nearby galactic supernova neutrino detection in RES-NOVA as proposed in our previous work [23]. Furthermore, our analyses indicate that there exist two categories of correlations among parameters: spectral-induced correlation and mixing-induced correlation. The former is encoded in the formalism of neutrino flux, while the latter derives from the complementary effects of neutrino mixing and detector configurations. Such correlations potentially offer us new ways to extract information from data, more efficiently, via specific combinations of spectral parameters. It is also possible to solve the mass ordering problem by analysing the mixing-induced correlations. However, more realistic oscillation models should be included in real observations, e.g., non-adiabatic oscillation, collective oscillation and Earth matter effect.

For future studies, an effective way to enhance the capability of our method is to further improve the flavour-blind sensitivity in the collections (e.g. higher statistics or extra sensitivity to neutrinos with energy below 10 MeV). For instance, the neutral current scatterings on ^{16}O in Hyper-K can provide valuable information in the low energy region (i.e., $5 \sim 10$ MeV), while the pES reaction in JUNO and neutral current scattering on Ar ($\nu + \text{Ar} \rightarrow \nu + \text{Ar}^*$) in DUNE (if available) will offer extra events in the relatively higher energy range. It is also worthy to mention that the next-generation large-scale dark matter detectors will also render complementary information in such studies (see, e.g., Ref [78, 79]). Nevertheless, both cross section and detector uncertainties should get treated properly in analysing the data from future realistic observations. Especially, the cross section uncertainties of $\nu\text{Ar}(\text{CC})$ can manifestly affect the results, as shown in our estimate (also see Ref [77]). The lack of proper treatment on such uncertainty information makes the spectral parameter uncertainties in the given results, to some extent, not realistic, which appears as one of the main limitations in this study. At last, we would like to note that a precise measurement of the distance to super-

nova is also of great importance, since that would lead to uncertainties on the determination of \mathcal{E}_ν (see eq. (2.4)).

A Flat prior

We replace the Gauss distributions (see, e.g., eq. (3.3)) with flat distributions, whose parameter spaces are restricted to the 3σ regions of Gauss distributions, in the analysis. Considering no neutrino oscillation, the results are presented in table 4 and figure 7. Generally speaking,

Table 4: The same as table 3, but flat priors are under estimate now. No neutrino oscillation is assumed.

Osc	estimate	α			$\langle E \rangle$ [MeV]			\mathcal{E} [10^{52} erg]		
		ν_e	$\bar{\nu}_e$	ν_x	ν_e	$\bar{\nu}_e$	ν_x	ν_e	$\bar{\nu}_e$	ν_x
NO	MAP	2.79	3.24	2.83	14.39	16.25	17.89	7.70	6.45	5.69
	$2\sigma^-$	-0.39	-0.09	-1.16	-0.73	-0.13	-2.22	-0.37	-0.06	-0.66
	$2\sigma^+$	+0.33	+0.09	+1.30	+0.57	+0.13	+2.54	+0.40	+0.06	+0.84
	%	12.9	2.8	43.5	4.5	0.8	13.3	5.0	0.9	13.2

the posterior distributions are quite similar to that of Gauss priors (see, e.g., table 3 and figure 3). The results of $\bar{\nu}_e$ flavour remain almost the same, due to the highly informative dataset offered by the IBD-p reaction in Hyper-K. The influence on the extraction of ν_e part are also tiny, i.e., only an increase of $\sim 0.3\%$ on the 2σ symmetrized fractional uncertainty. However, such replacement shows relatively noticeable impact on the retrieval of ν_x component, namely an increase of 10.1% on α and enlargement of $\sim 2.5\%$ on $\langle E \rangle$ and \mathcal{E} . Such consequences are totally reasonable, and confirm the previous statement that the more informative the dataset is, the less dependence the posterior will show on the prior. Note that these priors can be further updated according to future developments on modelling of stellar core collapse.

Acknowledgments

We are grateful to Ming-chung Chu for useful comments. X.-R. Huang acknowledges support from Shanghai Jiao Tong University via the Fellowship of Outstanding PhD Graduates. This work was supported in part by the National Natural Science Foundation of China under Grant Nos. 12235010 and 11625521, and the National SKA Program of China No. 2020SKA0120300.

Note added. The data and code underlying this article will be shared on reasonable request.

References

- [1] KAMIOKANDE-II collaboration, *Observation of a Neutrino Burst from the Supernova SN 1987a*, *Phys. Rev. Lett.* **58** (1987) 1490.
- [2] R.M. Bionta et al., *Observation of a Neutrino Burst in Coincidence with Supernova SN 1987a in the Large Magellanic Cloud*, *Phys. Rev. Lett.* **58** (1987) 1494.

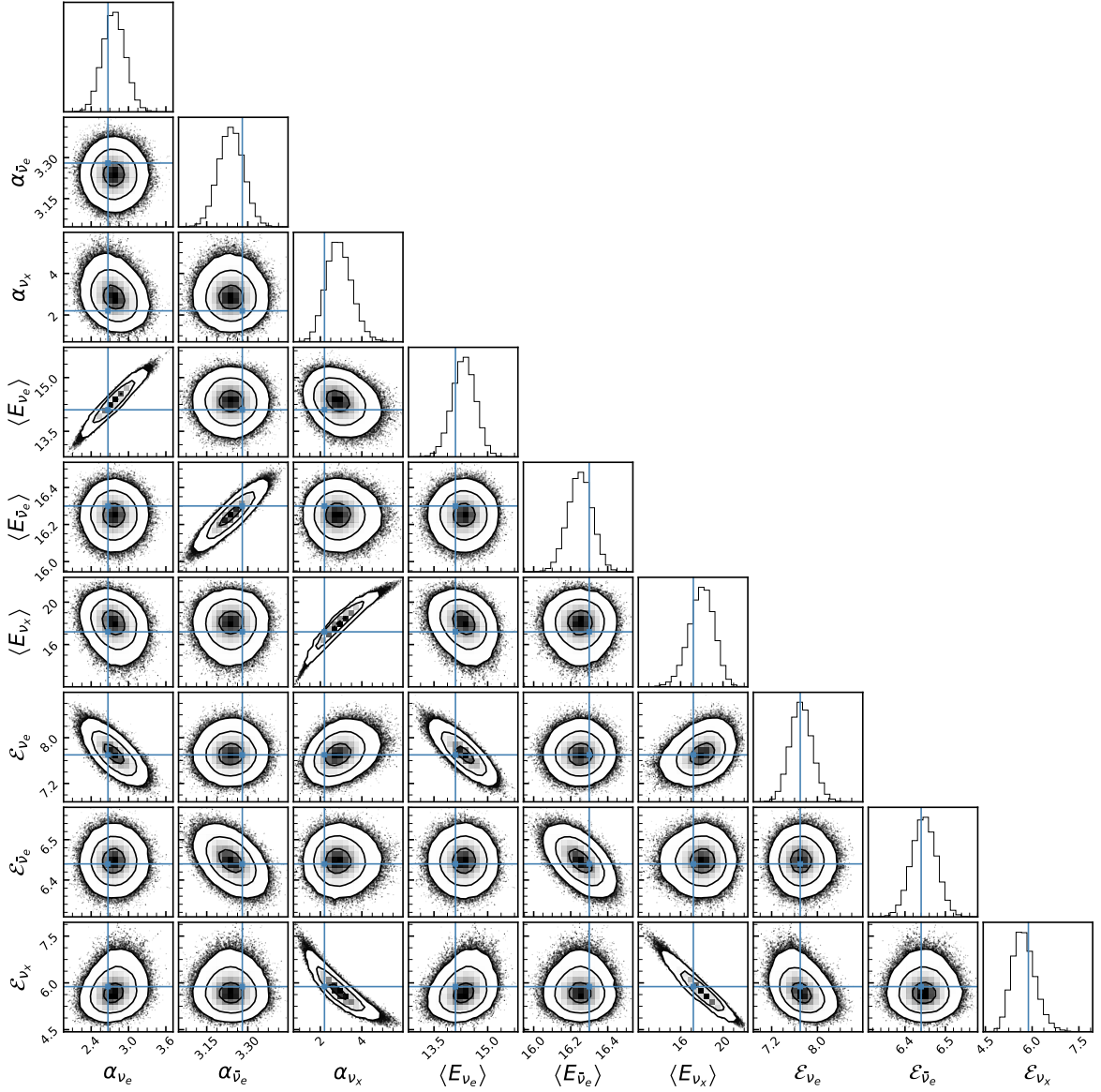


Figure 7: The same as figure 3, but the flat prior distributions are involved.

- [3] E. Alexeyev, L. Alexeyeva, I. Krivosheina and V. Volchenko, *Detection of the neutrino signal from sn 1987a in the lmc using the inr baksan underground scintillation telescope*, *Physics Letters B* **205** (1988) 209.
- [4] K. Sato and H. Suzuki, *Analysis of Neutrino Burst From the Supernova in LMC*, *Phys. Rev. Lett.* **58** (1987) 2722.
- [5] A. Burrows and J.M. Lattimer, *Neutrinos from SN 1987A*, *Astrophys. J. Lett.* **318** (1987) L63.
- [6] W.D. Arnett and J.L. Rosner, *Neutrino Mass Limits From Sn1987a*, *Phys. Rev. Lett.* **58** (1987) 1906.
- [7] J.N. Bahcall, T. Piran, W.H. Press and D.N. Spergel, *Neutrino Temperatures and Fluxes From the LMC Supernova*, *Nature* **327** (1987) 682.
- [8] T.J. Loredo and D.Q. Lamb, *Neutrino from SN1987A: Implications for cooling of the nascent*

- neutron star and the mass of the electron anti-neutrino, *Annals N. Y. Acad. Sci.* **571** (1989) 601.
- [9] T.J. Loredo and D.Q. Lamb, *Bayesian analysis of neutrinos observed from supernova SN-1987A*, *Phys. Rev. D* **65** (2002) 063002 [[astro-ph/0107260](#)].
- [10] H.A. Bethe, *Supernova mechanisms*, *Rev. Mod. Phys.* **62** (1990) 801.
- [11] H.-T. Janka, *Explosion Mechanisms of Core-Collapse Supernovae*, *Ann. Rev. Nucl. Part. Sci.* **62** (2012) 407 [[1206.2503](#)].
- [12] B. Müller, *The Status of Multi-Dimensional Core-Collapse Supernova Models*, *Publ. Astron. Soc. Austral.* **33** (2016) e048 [[1608.03274](#)].
- [13] E. O'Connor et al., *Global Comparison of Core-Collapse Supernova Simulations in Spherical Symmetry*, *J. Phys. G* **45** (2018) 104001 [[1806.04175](#)].
- [14] O. Just, R. Bollig, H.-T. Janka, M. Obergaulinger, R. Glas and S. Nagataki, *Core-collapse supernova simulations in one and two dimensions: comparison of codes and approximations*, *Mon. Not. Roy. Astron. Soc.* **481** (2018) 4786 [[1805.03953](#)].
- [15] A. Burrows and D. Vartanyan, *Core-Collapse Supernova Explosion Theory*, *Nature* **589** (2021) 29 [[2009.14157](#)].
- [16] Z.-z. Xing, *Flavor structures of charged fermions and massive neutrinos*, *Phys. Rept.* **854** (2020) 1 [[1909.09610](#)].
- [17] K. Scholberg, *Supernova Neutrino Detection*, *Ann. Rev. Nucl. Part. Sci.* **62** (2012) 81 [[1205.6003](#)].
- [18] U. Mosel, *Neutrino Interactions with Nucleons and Nuclei: Importance for Long-Baseline Experiments*, *Ann. Rev. Nucl. Part. Sci.* **66** (2016) 171 [[1602.00696](#)].
- [19] B. Dutta and L.E. Strigari, *Neutrino physics with dark matter detectors*, *Ann. Rev. Nucl. Part. Sci.* **69** (2019) 137 [[1901.08876](#)].
- [20] A. Mirizzi, I. Tamborra, H.-T. Janka, N. Saviano, K. Scholberg, R. Bollig et al., *Supernova Neutrinos: Production, Oscillations and Detection*, *Riv. Nuovo Cim.* **39** (2016) 1 [[1508.00785](#)].
- [21] S. Horiuchi and J.P. Kneller, *What can be learned from a future supernova neutrino detection?*, *J. Phys. G* **45** (2018) 043002 [[1709.01515](#)].
- [22] B. Müller, *Neutrino Emission as Diagnostics of Core-Collapse Supernovae*, *Ann. Rev. Nucl. Part. Sci.* **69** (2019) 253 [[1904.11067](#)].
- [23] X.-R. Huang and L.-W. Chen, *Supernova neutrinos as a precise probe of nuclear neutron skin*, *Phys. Rev. D* **106** (2022) 123034 [[2210.04534](#)].
- [24] B. Chauhan, *Using supernova neutrinos to probe strange spin of proton with JUNO and THEIA*, [2211.08443](#).
- [25] S. Baum, F. Capozzi and S. Horiuchi, *Rocks, water, and noble liquids: Unfolding the flavor contents of supernova neutrinos*, *Phys. Rev. D* **106** (2022) 123008 [[2203.12696](#)].
- [26] E.P. O'Connor and S.M. Couch, *Exploring Fundamentally Three-dimensional Phenomena in High-fidelity Simulations of Core-collapse Supernovae*, *Astrophys. J.* **865** (2018) 81 [[1807.07579](#)].
- [27] A. Burrows, D. Radice, D. Vartanyan, H. Nagakura, M.A. Skinner and J. Dolence, *The Overarching Framework of Core-Collapse Supernova Explosions as Revealed by 3D Fornax Simulations*, *Mon. Not. Roy. Astron. Soc.* **491** (2020) 2715 [[1909.04152](#)].
- [28] H. Nagakura, A. Burrows, D. Vartanyan and D. Radice, *Core-collapse supernova neutrino emission and detection informed by state-of-the-art three-dimensional numerical models*, *Mon. Not. Roy. Astron. Soc.* **500** (2020) 696 [[2007.05000](#)].

- [29] HYPER-KAMIOKANDE collaboration, *Hyper-Kamiokande Design Report*, [1805.04163](#).
- [30] ICECUBE collaboration, *IceCube Sensitivity for Low-Energy Neutrinos from Nearby Supernovae*, *Astron. Astrophys.* **535** (2011) A109 [[1108.0171](#)].
- [31] JUNO collaboration, *Neutrino Physics with JUNO*, *J. Phys. G* **43** (2016) 030401 [[1507.05613](#)].
- [32] THEIA collaboration, *THEIA: an advanced optical neutrino detector*, *Eur. Phys. J. C* **80** (2020) 416 [[1911.03501](#)].
- [33] DUNE collaboration, *Deep Underground Neutrino Experiment (DUNE), Far Detector Technical Design Report, Volume I Introduction to DUNE*, *JINST* **15** (2020) T08008 [[2002.02967](#)].
- [34] DUNE collaboration, *Deep Underground Neutrino Experiment (DUNE), Far Detector Technical Design Report, Volume II: DUNE Physics*, [2002.03005](#).
- [35] DUNE collaboration, *Supernova neutrino burst detection with the Deep Underground Neutrino Experiment*, *Eur. Phys. J. C* **81** (2021) 423 [[2008.06647](#)].
- [36] L. Pattavina, N. Ferreiro Iachellini and I. Tamborra, *Neutrino observatory based on archaeological lead*, *Phys. Rev. D* **102** (2020) 063001 [[2004.06936](#)].
- [37] RES-NOVA collaboration, *RES-NOVA sensitivity to core-collapse and failed core-collapse supernova neutrinos*, *JCAP* **10** (2021) 064 [[2103.08672](#)].
- [38] K. Rozwadowska, F. Vissani and E. Cappellaro, *On the rate of core collapse supernovae in the milky way*, *New Astron.* **83** (2021) 101498 [[2009.03438](#)].
- [39] R. Laha and J.F. Beacom, *Gadolinium in water Cherenkov detectors improves detection of supernova ν_e* , *Phys. Rev. D* **89** (2014) 063007 [[1311.6407](#)].
- [40] A. Nikrant, R. Laha and S. Horiuchi, *Robust measurement of supernova ν_e spectra with future neutrino detectors*, *Phys. Rev. D* **97** (2018) 023019 [[1711.00008](#)].
- [41] B. Dasgupta and J.F. Beacom, *Reconstruction of supernova ν_μ , ν_τ , anti- ν_μ , and anti- ν_τ neutrino spectra at scintillator detectors*, *Phys. Rev. D* **83** (2011) 113006 [[1103.2768](#)].
- [42] J.-S. Lu, Y.-F. Li and S. Zhou, *Getting the most from the detection of Galactic supernova neutrinos in future large liquid-scintillator detectors*, *Phys. Rev. D* **94** (2016) 023006 [[1605.07803](#)].
- [43] A. Gallo Rosso, F. Vissani and M.C. Volpe, *What can we learn on supernova neutrino spectra with water Cherenkov detectors?*, *JCAP* **04** (2018) 040 [[1712.05584](#)].
- [44] A. Gallo Rosso, *Supernova neutrino fluxes in HALO-1kT, Super-Kamiokande, and JUNO*, *JCAP* **06** (2021) 046 [[2012.12579](#)].
- [45] H.-L. Li, Y.-F. Li, M. Wang, L.-J. Wen and S. Zhou, *Towards a complete reconstruction of supernova neutrino spectra in future large liquid-scintillator detectors*, *Phys. Rev. D* **97** (2018) 063014 [[1712.06985](#)].
- [46] H.-L. Li, X. Huang, Y.-F. Li, L.-J. Wen and S. Zhou, *Model-independent approach to the reconstruction of multiflavor supernova neutrino energy spectra*, *Phys. Rev. D* **99** (2019) 123009 [[1903.04781](#)].
- [47] H. Nagakura, *Retrieval of energy spectra for all flavours of neutrinos from core-collapse supernova with multiple detectors*, *Mon. Not. Roy. Astron. Soc.* **500** (2020) 319 [[2008.10082](#)].
- [48] M.T. Keil, G.G. Raffelt and H.-T. Janka, *Monte Carlo study of supernova neutrino spectra formation*, *Astrophys. J.* **590** (2003) 971 [[astro-ph/0208035](#)].
- [49] I. Tamborra, B. Muller, L. Hudepohl, H.-T. Janka and G. Raffelt, *High-resolution supernova neutrino spectra represented by a simple fit*, *Phys. Rev. D* **86** (2012) 125031 [[1211.3920](#)].

- [50] G. D'Agostini, *Bayesian inference in processing experimental data: Principles and basic applications*, *Rept. Prog. Phys.* **66** (2003) 1383 [[physics/0304102](#)].
- [51] G. Ashton et al., *BILBY: A user-friendly Bayesian inference library for gravitational-wave astronomy*, *Astrophys. J. Suppl.* **241** (2019) 27 [[1811.02042](#)].
- [52] J.E. Bernhard, J.S. Moreland, S.A. Bass, J. Liu and U. Heinz, *Applying Bayesian parameter estimation to relativistic heavy-ion collisions: simultaneous characterization of the initial state and quark-gluon plasma medium*, *Phys. Rev. C* **94** (2016) 024907 [[1605.03954](#)].
- [53] R. Trotta, *Bayes in the sky: Bayesian inference and model selection in cosmology*, *Contemp. Phys.* **49** (2008) 71 [[0803.4089](#)].
- [54] T.J. Loredo, *Bayesian astrostatistics: a backward look to the future*, [1208.3036](#).
- [55] K. Scholberg, *Supernova Signatures of Neutrino Mass Ordering*, *J. Phys. G* **45** (2018) 014002 [[1707.06384](#)].
- [56] HYPER-KAMIOKANDE collaboration, *Supernova Model Discrimination with Hyper-Kamiokande*, *Astrophys. J.* **916** (2021) 15 [[2101.05269](#)].
- [57] X.-R. Huang and L.-W. Chen, *Neutron Skin in CsI and Low-Energy Effective Weak Mixing Angle from COHERENT Data*, *Phys. Rev. D* **100** (2019) 071301 [[1902.07625](#)].
- [58] PREX collaboration, *Accurate Determination of the Neutron Skin Thickness of ^{208}Pb through Parity-Violation in Electron Scattering*, *Phys. Rev. Lett.* **126** (2021) 172502 [[2102.10767](#)].
- [59] COHERENT collaboration, *Observation of Coherent Elastic Neutrino-Nucleus Scattering*, *Science* **357** (2017) 1123 [[1708.01294](#)].
- [60] COHERENT collaboration, *COHERENT Collaboration data release from the first observation of coherent elastic neutrino-nucleus scattering*, [1804.09459](#).
- [61] E. O'Connor and C.D. Ott, *The progenitor dependence of the pre-explosion neutrino emission in core-collapse supernovae*, *Astrophys. J.* **762** (2012) 126.
- [62] S. Seadrow, A. Burrows, D. Vartanyan, D. Radice and M.A. Skinner, *Neutrino Signals of Core-Collapse Supernovae in Underground Detectors*, *Mon. Not. Roy. Astron. Soc.* **480** (2018) 4710 [[1804.00689](#)].
- [63] K.-C. Pan, M. Liebendörfer, S.M. Couch and F.-K. Thielemann, *Equation of State Dependent Dynamics and Multi-messenger Signals from Stellar-mass Black Hole Formation*, *Astrophys. J.* **857** (2018) 13 [[1710.01690](#)].
- [64] A. da Silva Schneider, E. O'Connor, E. Granqvist, A. Betranhandy and S.M. Couch, *Equation of State and Progenitor Dependence of Stellar-mass Black Hole Formation*, *Astrophys. J.* **894** (2020) 4 [[2001.10434](#)].
- [65] A.R. Raduta, F. Nacu and M. Oertel, *Equations of state for hot neutron stars*, *Eur. Phys. J. A* **57** (2021) 329 [[2109.00251](#)].
- [66] H. Minakata, H. Nunokawa, R. Tomas and J.W.F. Valle, *Parameter Degeneracy in Flavor-Dependent Reconstruction of Supernova Neutrino Fluxes*, *JCAP* **12** (2008) 006 [[0802.1489](#)].
- [67] W. Liao, *Detecting supernovae neutrino with Earth matter effect*, *Phys. Rev. D* **94** (2016) 113016 [[1607.03334](#)].
- [68] E.K. Akhmedov, C. Lunardini and A.Y. Smirnov, *Supernova neutrinos: Difference of muon-neutrino - tau-neutrino fluxes and conversion effects*, *Nucl. Phys. B* **643** (2002) 339 [[hep-ph/0204091](#)].
- [69] A.B. Balantekin, J. Gava and C. Volpe, *Possible CP-Violation effects in core-collapse Supernovae*, *Phys. Lett. B* **662** (2008) 396 [[0710.3112](#)].

- [70] PARTICLE DATA GROUP collaboration, *Review of Particle Physics*, *PTEP* **2022** (2022) 083C01.
- [71] L. Hudepohl, B. Muller, H.T. Janka, A. Marek and G.G. Raffelt, *Neutrino Signal of Electron-Capture Supernovae from Core Collapse to Cooling*, *Phys. Rev. Lett.* **104** (2010) 251101 [0912.0260].
- [72] D. Foreman-Mackey, D.W. Hogg, D. Lang and J. Goodman, *emcee: The MCMC Hammer*, *Publ. Astron. Soc. Pac.* **125** (2013) 306 [1202.3665].
- [73] M. Mukhopadhyay, C. Lunardini, F.X. Timmes and K. Zuber, *Presupernova neutrinos: directional sensitivity and prospects for progenitor identification*, *Astrophys. J.* **899** (2020) 153 [2004.02045].
- [74] D. Foreman-Mackey, *corner.py: Scatterplot matrices in python*, *The Journal of Open Source Software* **1** (2016) 24.
- [75] M.-K. Cheoun, E. Ha and T. Kajino, *Reactions on Ar-40 involving solar neutrinos and neutrinos from core-collapsing supernovae*, *Phys. Rev. C* **83** (2011) 028801.
- [76] T. Suzuki and M. Honma, *Neutrino Capture Reactions on ^{40}Ar* , *Phys. Rev. C* **87** (2013) 014607 [1211.4078].
- [77] DUNE collaboration, *Impact of cross-section uncertainties on supernova neutrino spectral parameter fitting in the Deep Underground Neutrino Experiment*, *Phys. Rev. D* **107** (2023) 112012 [2303.17007].
- [78] R.F. Lang, C. McCabe, S. Reichard, M. Selvi and I. Tamborra, *Supernova neutrino physics with xenon dark matter detectors: A timely perspective*, *Phys. Rev. D* **94** (2016) 103009 [1606.09243].
- [79] DARKSIDE 20K collaboration, *Sensitivity of future liquid argon dark matter search experiments to core-collapse supernova neutrinos*, *JCAP* **03** (2021) 043 [2011.07819].